Semiclassical bounds on the dynamics of two-dimensional interacting disordered fermions

Łukasz Iwanek [●],[1] Marcin Mierzejewski [●],[1] Anatoli Polkovnikov [●],[2] Dries Sels,[3,4] and Adam S. Sajna [●][1]

[1]*Institute of Theoretical Physics, Faculty of Fundamental Problems of Technology,*
Wrocław University of Science and Technology, 50-370 Wrocław, Poland
[2]*Department of Physics, Boston University, 590 Commonwealth Avenue, Boston, Massachusetts 02215, USA*
[3]*Department of Physics, New York University, New York, New York 10003, USA*
[4]*Center for Computational Quantum Physics, Flatiron Institute, New York, New York 10010, USA*

Using the truncated Wigner approximation (TWA) we study quench dynamics of two-dimensional lattice systems consisting of interacting spinless fermions with potential disorder. First, we demonstrate that the semiclassical dynamics generally relaxes faster than the full quantum dynamics. We obtain this result by comparing the semiclassical dynamics with exact diagonalization and Lanczos propagation of one-dimensional chains. Next, exploiting the TWA capabilities of simulating large lattices, we investigate how the relaxation rates depend on the dimensionality of the studied system. We show that strongly disordered one-dimensional and two-dimensional systems exhibit a transient, logarithmic-in-time relaxation, which was recently established for one-dimensional chains. Such relaxation corresponds to the infamous $1/f$ noise at strong disorder.

I. INTRODUCTION

Anomalous dynamics of strongly disordered systems with many-body interactions has recently attracted significant interest leading to numerous experimental and theoretical studies. The problem emerged from studying the role of electron-electron interactions in the fate of the Anderson localization of noninteracting particles [1,2]. Numerical studies of one-dimensional (1D) chains indicated that, at sufficiently strong disorder, interacting finite-size systems remain localized or nearly localized even in the presence of local two-body interactions [3–20]. The ultimate stability of the many-body localization (MBL) in macroscopic systems is under debate [21–25] and it has been questioned in a series of recent works [26–30]. However, it is well established that at strong disorder interacting chains exhibit very slow logarithmic-in-time relaxation [31–56]. Such slow dynamics in one dimension was also found in systems where the noninteracting limit does not correspond to the localized phase [42,48,57,58]. The finite-time dynamics of strongly disordered systems is typically subdiffusive [15,41,59–64]. Such slow dynamics was frequently considered as a precursor to localization [15,41,59–64] and was attributed to the Griffiths effects due to the presence of weak links responsible for the existence of rare localized regions [39,47,65,66].

Despite the localized phase in the thermodynamic limit being likely unstable to interactions, there is a key open question about long-time dynamics in such systems. Existing computational methods have severe limitations on accessible system sizes and/or accessible timescales. Due to these limitations, previous numerical studies focused mainly on the dynamics of 1D finite-size systems. At the same time, several recent experiments show signatures that drastic slowing down of dynamics

at large disorder also exists in two-dimensional (2D) systems [47,67,68] and three-dimensional systems [69]. Theoretically, dynamics of strongly disordered systems beyond 1D remains largely an open problem [70,71].

In this paper, we demonstrate that the semiclassical description in terms of the fermionic truncated Wigner approximation (fTWA) [72–77] allows one to partially overcome the limitations of other numerical methods and analyze long-time dynamics both in 1D and in 2D systems. While the semiclassical approach is not expected to be quantitatively reliable at long times, namely it leads to faster relaxation dynamics than seen within exact numerical methods, it shows qualitative agreement with exact dynamics in 1D systems. At the same time, fTWA allows one to overcome small size, short time, and dimensionality limitations intrinsic to other methods because the complexity of the fTWA calculations scales only polynomially with the system size. Utilizing this approach, we show for strongly disordered 2D systems that the imbalance decays logarithmically in time, characteristic of glassy behavior. Because fTWA gives a faster decay than in actual systems, this result implies that the decay should also be at most logarithmic in time. Such logarithmic time dependence is reflected in the spectral functions showing approximate $1/\omega$ dependence also established in 1D disordered systems [28,42,78,79]. The emergence of such an inverse frequency spectral function form, at least within fTWA, is thus not special to 1D systems. We note that this form of the spectral function is also known as $1/f$ noise, which was observed experimentally in a broad range of physical systems [80].

The remainder of this paper is organized as follows: in Sec. II we introduce the disordered spinless fermionic model and the implementation of the fTWA method. In Sec. III we show how fTWA bounds the actual decay of correlations in

quantum systems. In Sec. IV we present an analysis of the relaxation dynamics and the spectral function, focusing on 2D systems. Finally we summarize our results. In the Appendices we show the analysis of finite-size effects on the system dynamics.

II. DYNAMICS OF SPINLESS FERMIONS WITHIN fTWA

In this work we consider spinless fermions whose dynamics is given by the following Hamiltonian:

$$\hat{H} = -J \sum_{\langle ij \rangle} (\hat{c}_i^\dagger \hat{c}_j + \text{H.c.}) + V \sum_{\langle ij \rangle} \left(\hat{n}_i - \frac{1}{2} \right) \left(\hat{n}_j - \frac{1}{2} \right)$$
$$+ \sum_i \Delta_i \left(\hat{n}_i - \frac{1}{2} \right), \tag{1}$$

where $\langle ij \rangle$ stands for nearest neighbor sites, $\hat{c}_i$ ($\hat{c}_i^\dagger$) is the fermionic annihilation (creation) operator on the site i, $\hat{n}_i = \hat{c}_i^\dagger \hat{c}_i$ is the corresponding number operator, J is the hoping amplitude, V is the nearest neighbor interaction coupling, and Δ_i is a local random potential drawn from a uniform distribution in the range $[-W, W]$.

We describe the dynamics of the electrons within the semiclassical fTWA method [72]. Within this framework, fermionic bilinears $\hat{E}_j^i = (\hat{c}_i^\dagger \hat{c}_j - \hat{c}_j \hat{c}_i^\dagger)/2$ are mapped to the complex phase space variables ρ_{ij} (e.g., $\hat{n}_i$ operator maps to $\rho_{ii} + 1/2$). The phase space variables satisfy the canonical Poisson bracket relations [81] with the structure constants given by the corresponding quantum commutation relations:

$$\left[\hat{E}_j^i, \hat{E}_l^k \right] = \hat{E}_l^i \delta_{kj} - \hat{E}_j^k \delta_{il} \rightarrow \{ \rho_{ij}, \rho_{kl} \} = \rho_{il} \delta_{kj} - \rho_{kj} \delta_{il}, \tag{2}$$

where $\rho_{ij} = \rho_{ji}^*$. We note that the operators $\hat{E}_j^i$ form a representation of a $su(N)$ algebra, where N is the number of sites. The operators are mapped to functions using the Wigner-Weyl quantization [82]. In particular, the Hamiltonian $\hat{H}$ is mapped to its Weyl symbol H_W:

$$H_W = J \sum_{\langle ij \rangle} (\rho_{ij} + \text{c.c.}) + \sum_i \left(\Delta_i \rho_{ii} + V \rho_{ii}^2 \right) + V \sum_{\langle ij \rangle} \rho_{ii} \rho_{jj}, \tag{3}$$

and the initial density matrix $\hat{\rho}^0$ is mapped to the Wigner function $\mathcal{W}(\{\rho_{ij}^0\})$, which plays the role of the initial probability distribution of the phase space variables [here, the following notation is used: $\rho_{kl}^0 \equiv \rho_{kl}(t=0)$]. The origin of $V \rho_{ii}^2$ in H_W is explained in Appendix A. The dynamics of the phase space variables within the fTWA is described by the classical Hamiltonian equations of motion:

$$i \frac{d\rho_{kl}}{dt} = \{ \rho_{kl}, H_W \} = \sum_m \left(\frac{\partial H_W}{\partial \rho_{lm}} \rho_{km} - \frac{\partial H_W}{\partial \rho_{mk}} \rho_{ml} \right). \tag{4}$$

To find an observable at the time, t, we need to evolve the phase space variables in time starting from initial conditions drawn from the Wigner function, compute the Weyl symbol of the corresponding operator, and then average over the initial conditions. In this paper we are focusing on the expectation values of the number operators, such that this prescription gives

$$\langle \hat{n}_i(t) \rangle \approx \int \left(\rho_{ii}(t) + \frac{1}{2} \right) W(\{\rho_{kl}^0\}) D\rho_{kl}^0, \tag{5}$$

where $D\rho_{kl}^0$ stands for integration over all independent phase space variables. In our simulations we use open boundary conditions and start from the initial states which are the product of single site states with 0 or 1 fermions. The latter allows us to approximate the initial Wigner function as a factorizable over different pairs of sites Gaussian distribution

$$\mathcal{W}(\{\rho_{kl}\}) = \prod_{kl} \frac{1}{2\pi \sigma_{kl}^2} \exp \left(\frac{(\rho_{kl} - \mu_{kl})(\rho_{kl}^* - \mu_{kl})}{2\sigma_{kl}^2} \right), \tag{6}$$

where μ_{kl} and σ_{kl} are fixed by the expectation values and the fluctuations of the operators $\hat{E}_j^i$ [72], i.e.,

$$\text{Tr}\left(\hat{\rho} \hat{E}_l^k \right) = \int \rho_{kl} \mathcal{W}(\{\rho_{mn}\}) D\rho_{mn}, \tag{7}$$

$$\frac{1}{2} \text{Tr}\left(\hat{\rho} \left(\hat{E}_j^i \hat{E}_l^k + \hat{E}_l^k \hat{E}_j^i \right) \right) = \int \rho_{ij} \rho_{kl} \mathcal{W}(\{\rho_{mn}\}) D\rho_{mn}. \tag{8}$$

Let us note that the complexity of the fTWA scales polynomially with the system size L as the dimensionality of the phase space, L^2, is much less than the dimensionality of the quantum Hilbert space 2^L. In the interacting systems, fTWA is guaranteed to be accurate only at early times [72,82], while in noninteracting systems fTWA is exact at all times. This method also becomes exact for fermions with infinite range interactions and, in particular, it can accurately describe dynamics of systems with long-range interactions [75]. It can also be made asymptotically exact by increasing the number of fermion flavors [77]. It is also expected that accuracy of fTWA increases with the dimensionality of the system.

III. FTWA AS A BOUND FOR RELAXATION DYNAMICS

Before we analyze 2D systems in this section we benchmark the applicability of fTWA in 1D systems by comparing it to exact diagonalization (ED) and the Lanczos method [83,84]. We consider quenches from an initial charge density wave (CDW) product state at half filling:

$$|\psi(t = 0)\rangle = |0\rangle|1\rangle|0\rangle|1\rangle \cdots, \tag{9}$$

where $|0\rangle$ and $|1\rangle$ are empty and occupied states which alternate between neighboring sites. Such states are accessible experimentally, e.g., they were realized in ultracold atom experiments [85–87]. They are easily represented by the approximate Wigner function in fTWA [72–77]. In simulations we analyze the imbalance function related to the on-site densities in the following way:

$$I(t) = \frac{N_o(t) - N_e(t)}{N_o(t) + N_e(t)}, \tag{10}$$

where

$$N_o(t) = \sum_{i \in \text{initially occupied sites}} \langle \hat{n}_i(t) \rangle, \tag{11}$$

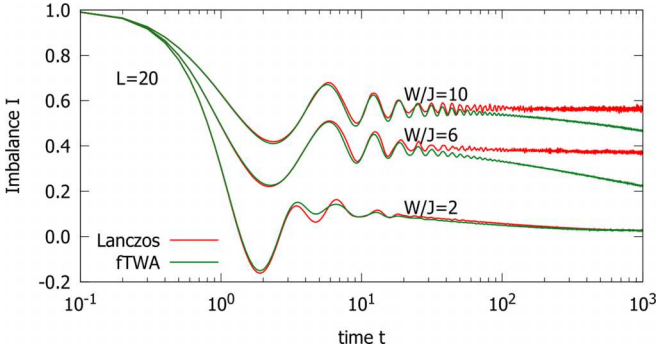$$N_e(t) = \sum_{i \in \text{initially empty sites}} \langle \hat{n}_i(t) \rangle. \tag{12}$$

FIG. 1. Time dependence of the imbalance for different disorder strengths W. Numerical calculations are performed for a 1D lattice with $L = 20$ sites. The fTWA and Lanczos data are represented by a green and red line, respectively. Data from top to bottom are obtained for disorders with strength $W/J = 10, 6, 2$, respectively, and are averaged over 200 disorders realizations. The rest of the parameters are $V/J = 1$, $J = 0.5$. In fTWA we use 500 trajectories for each disorder realization.

This imbalance was widely used both in ultracold atom experiments [47,67,85,86,88] and in numerical simulations [23] as an indicator of thermalization. In Fig. 1 we show the time dependence of the imbalance $I(t)$ computed within the fTWA and the Lanczos methods starting from the CDW state in a 1D system of size $L = 20$. We set interaction strength $V = J$. We see that at short and intermediate times the fTWA accurately describes the imbalance, correctly predicting the initial transient dynamics followed by a crossover to a slow relaxation at strong disorder. At weaker disorder $W/J \lesssim 2$, the fTWA nearly agrees with the exact dynamics at all times. However at $W/J > 2$, we see that the fTWA predicts faster decay of the disorder-averaged imbalance over a long time. Interestingly, as the disorder keeps increasing the fTWA starts improving again, successively approaching the imbalance plateau (compare the results for $W/J = 6$ and $W/J = 10$ in Fig. 1). This behavior is consistent with previous observations in disordered spin systems [89,90] and in the long-range Hubbard model [75].

From recent literature [75,89,90], it can be concluded that, in comparison to the exact numerics, nonlinearities presented in the semiclassical description are responsible for the faster disappearance of the memory effects encoded in the initial

state of disordered systems. Here we show that this condition obtained previously for disorder averages holds for almost every single disorder realization. For long-time simulations we compare time averages of fTWA and ED imbalances in the time window $t \in (1000, 5000)$:

$$\tilde{I}^s_{\text{fTWA/ED}} = \frac{1}{\Delta t} \int_{t_0}^{t_0 + \Delta t} I^s_{\text{fTWA/ED}}(t) dt, \qquad (13)$$

where $t_0 = 1000$, $\Delta t = 4000$ and s index denotes that imbalance is calculated for single disorder realization. For larger disorder strengths points $(\tilde{I}^s_{\text{ED}}, \tilde{I}^s_{\text{fTWA}})$ are plotted in Figs. 2(a) and 2(b). We observe that the majority of points satisfy $\tilde{I}^s_{\text{fTWA}} \leqslant \tilde{I}^s_{\text{ED}}$, which suggest that fTWA dynamics can be regarded as an upper bound for relaxation rates. While we observe some violations of the proposed bound, we note a steady decrease of the number of disorder realizations with system size that do so; see insets in Figs. 2(a) and 2(b). Consequently, we expect a negligible effect of these rare realizations for the much larger systems studied in the next section.

We also check that the statistical uncertainty of $\tilde{I}^s_{\text{ED}}$ for the most upper point in Fig. 2(b), which satisfies $\tilde{I}^s_{\text{fTWA}} > \tilde{I}^s_{\text{ED}}$, coincides with $\tilde{I}^s_{\text{fTWA}} \approx \tilde{I}^s_{\text{ED}}$ condition within two standard deviations (2σ); see Fig. 2(c). The definition of σ is given by

$$\sigma^2 = \frac{1}{\Delta t} \int_{t_0}^{t_0 + \Delta t} \left(I^s_{\text{ED}}(t) - \tilde{I}^s_{\text{ED}} \right)^2 dt. \qquad (14)$$

IV. SPECTRAL FUNCTION IN 1D AND 2D LATTICES

To achieve further insight into the relaxation dynamics, it is convenient to analyze the spectral function defined as the Fourier transform of the imbalance function $I(t)$,

$$S(\omega) = \int_{-\infty}^{\infty} I(t) e^{-i\omega t} dt = 2 \text{Re} \left[\int_{0}^{\infty} I(t) e^{-i\omega t} dt \right]. \qquad (15)$$

First, we focus on the 1D system. Using data presented in Fig. 1, $S(\omega)$ is calculated for exact and fTWA imbalance; see Fig. 3. From obtained data, fTWA for the weak disorder strength ($W/J = 2$) is almost exact. For larger values of W/J, fTWA reflects ED results quantitatively down to ω of order $\mathcal{O}(10^{-1})$. Interestingly, for larger values of disorder strength, fTWA predicts almost $1/\omega$ behavior, which was also observed in other works [28,42,78,79]. Such nontrivial behavior
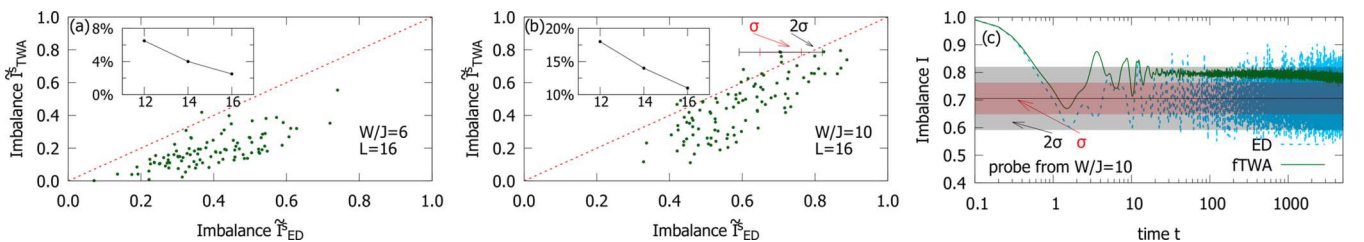

FIG. 2. Location of $(\tilde{I}^s_{\text{fTWA}}, \tilde{I}^s_{\text{ED}})$ points for 100 disorder realizations [(a) and (b)]. Panel (a) corresponds to $W/J = 6$ and panel (b) to $W/J = 10$. $\tilde{I}^s_{\text{fTWA/ED}}$ are calculated from averaging imbalances in time window $t \in (1000, 5000)$; see Eq. (13). The initial state is CDW with 16 lattice sites and, due to long-time dynamics, exact diagonalization method was used. Panel (c) represents one (σ) and two standard deviations (2σ) of ED data with respect to fTWA dynamics for the most upper point in (b). The insets in (a) and (b) show percentage of points satisfying the $\tilde{I}^s_{\text{fTWA}} > \tilde{I}^s_{\text{ED}}$ condition (vertical axis) when the system size (horizontal axis) is varied from 12 to 16 lattice sites (in calculations 200 disorder realizations were used). For fTWA 500 trajectories were used and the interaction strength was set to $V/J = 1$ with $J = 0.5$.
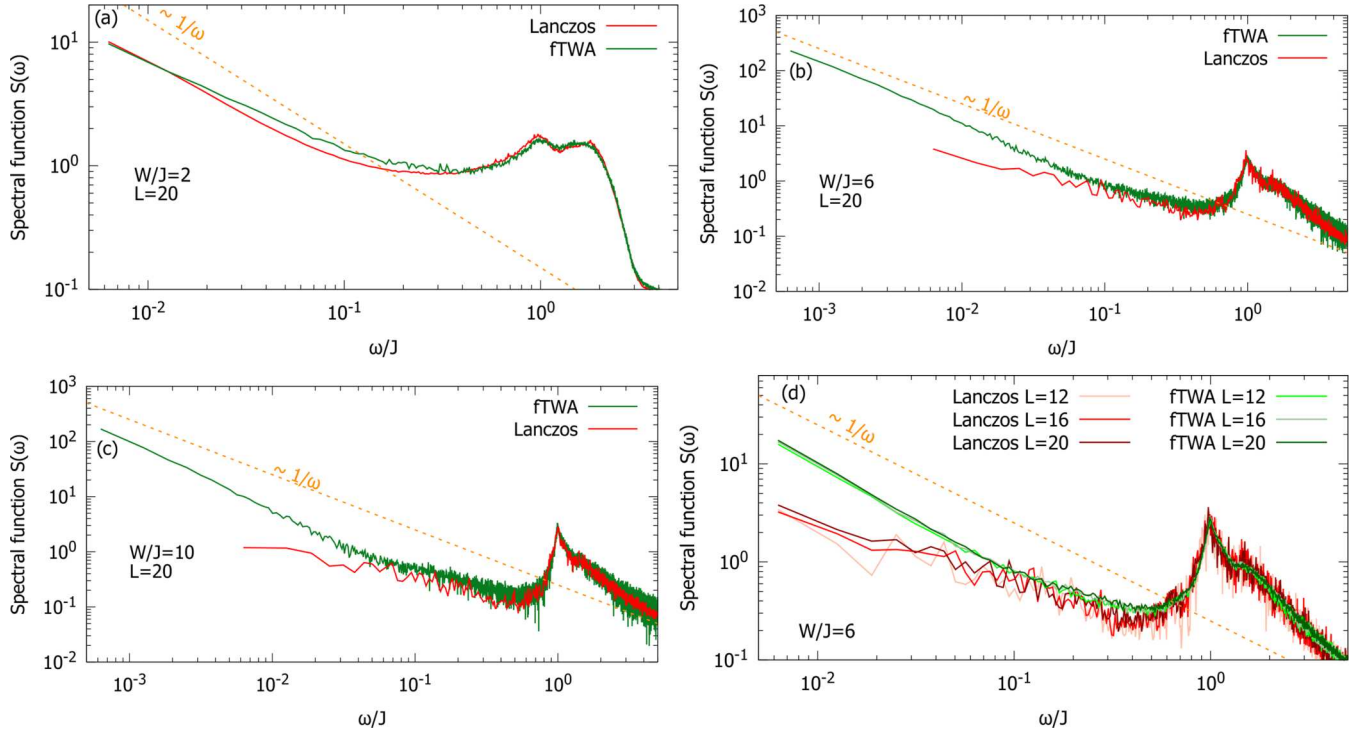
FIG. 3. (a)–(c) Spectral function $S(\omega)$ in a 1D system with $L = 20$ lattice sites. Disorder strength is set to (a) $W/J = 2$, (b) $W/J = 6$, (c) $W/J = 10$. Results for fTWA and Lanczos method (a)–(c) are shown as a green and red line, respectively. In (d), lattice sizes $L = 12, 16,$ 20 are plotted. The fTWA parameters are as follows: (a) and (d) 500 trajectories, (b) and (c) 400 trajectories due to long computation time requirements. In (a), (b), and (d) averaging over 200 disorders is taken while in (c) the number of disorder realizations is increased to 1000 in order to avoid noisy Lanczos data at strong disorder strength $W/J = 10$.

comes from logarithmic-in-time decay of the imbalance and is also partially visible in the propagation within the Lanczos method. These results suggest that fTWA upper bound for relaxation rates is of logarithmic type.

Moreover, analyzing finite-size effects of $S(\omega)$ in Fig. 3(d), we observe that in Lanczos simulations the spectral function weakly drifts to $1/\omega$ while the change in fTWA is negligible. For a more accurate comparison, lattice sites at boundaries were removed symmetrically when system sizes were decreased from $L = 20$ to $L = 12$ without changing the disorder distribution of the remaining sites.

As the main result of this work, we focus on the 2D systems in which fTWA is capable of simulating larger system sizes. We consider the initial product state of densities in the form of stripes [see inset in Fig. 4(a)]. Such stripelike structures are directly accessible in experiments [47,86]. In this work we simulate numerically 8×8 lattice sites in the long-time limit; see Fig. 4. As in the 1D system, we also observe logarithmic-in-time decay of imbalances which is also reflected in its spectral functions as $1/\omega$ dependence [Fig. 4(b)]. Due to the higher value of the coordination number in a 2D lattice we do not observe a sharp resonant feature around $\omega/J \approx 1$.
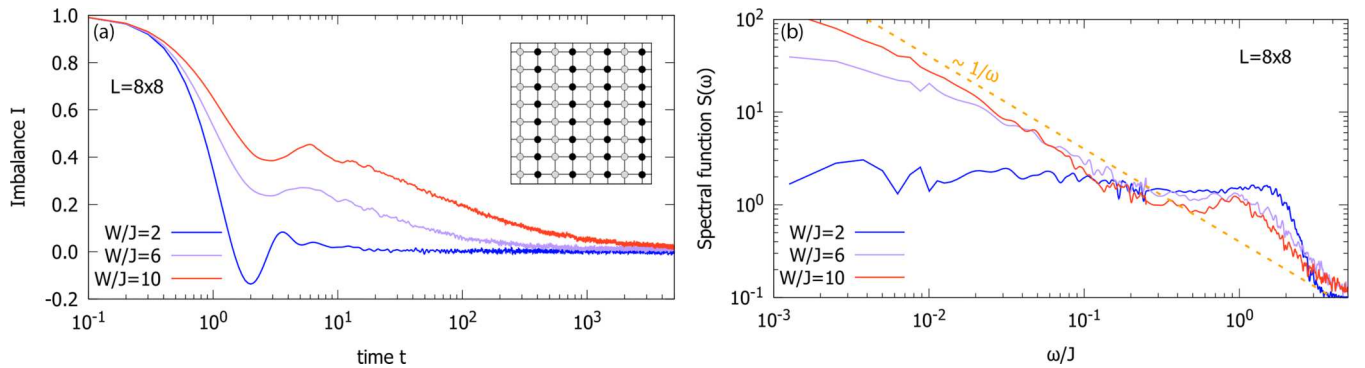

FIG. 4. Time dependence of imbalance (a) and spectral function $S(\omega)$ (b) in a 2D system with the size 8×8. The inset in (a) represents striped CDW initial condition (black circles represent occupied sites and white empty). Results represent data for fTWA with disorder strength $W/J = 2, 6, 10$, where the average over 30 disorder realizations was used. In fTWA there are 25 trajectories simulated for each disorder realization. The rest of the parameters are $V/J = 1, J = 0.5$.
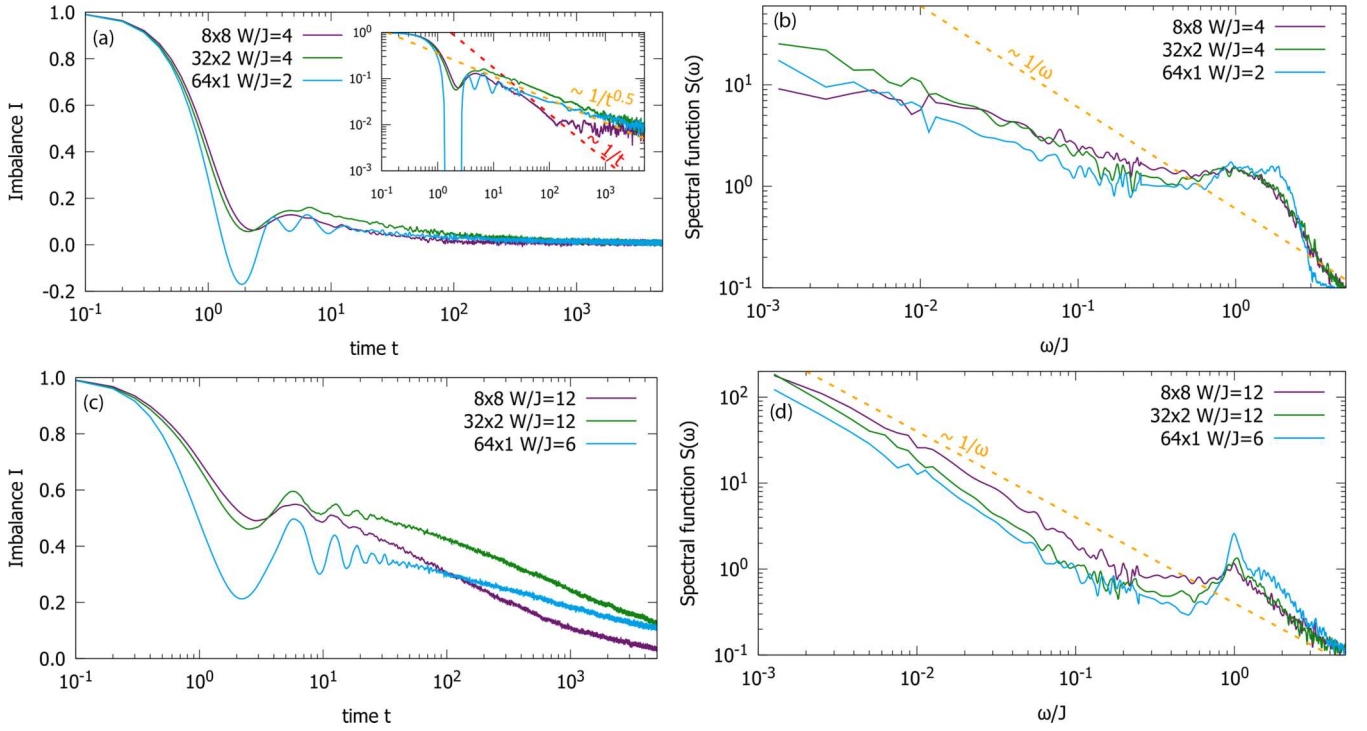
FIG. 5. Time dependence of imbalance [(a) and (c)] and spectral function $S(\omega)$ [(b) and (d)] for different lattice geometries 64×1 (finite 1D lattice), 8×8 (finite 2D lattice), and 32×2 (crossover region between 1D and 2D). Data for (a) and (b) represent disorder strength $W/J = 2$ for 1D, $W/J = 4$ for 2D and ladder type. Results for (c) and (d) represent disorder strength $W/J = 6$ for 1D, $W/J = 12$ for 2D and ladder type. For better comparison of 1D and 2D data, the disorder strength is doubled for 2D case. Each line is averaged over 30 disorder realization. In fTWA there are 25 trajectories for each disorder realization. Moreover, in the inset of (a), the same data as in (a) are presented but with the additional logarithmic scale on the vertical axis. The rest of the parameters are $V/J = 1$, $J = 0.5$.

To compare the crossover region between the 1D and 2D system we simulated 64×1, 32×2, 8×8 lattice sizes (see also finite-size effects analysis in Appendix B). Data obtained for imbalances together with their spectral functions are plotted in Fig. 5. To more efficiently compare data for different lattices, the disorder strength in 2D is set to two times larger value than in 1D. We observe that for the weaker disorder strengths [Fig. 5(a)] decay of imbalance at long times follows diffusive behavior, i.e., $I \sim 1/t^{0.5}$ in 1D and $I \sim 1/t$ in 2D. Therefore $1/\omega$ behavior is naturally not achieved in the spectral function analysis presented in Fig. 5(b). However, for the larger strengths of disorder, we observe that $1/\omega$ behavior emerges and is immune to the shape of the lattice [see Fig. 5(d)]. This confirms the universal $1/\omega$ behavior for interacting, strongly disordered systems.

Interestingly, obtained data also show that it is enough to consider a ladder-type lattice to observe almost two-dimensional behavior of the spectral function [compare Figs. 6(b) and 6(c). However, proper scaling of disorder strength with lattice dimension shows that the role of dimensionality is limited; see Figs. 5(b) and 5(d).

In this section all presented data for $S(\omega)$ starting from Fig. 4 and data in the inset of Fig. 5 have been passed through a Kaiser filter to remove some of the noise coming mostly from sampling of the initial Wigner function (for comparison of data with and without a filtered noise see Fig. 7 and the discussion in Appendix C).
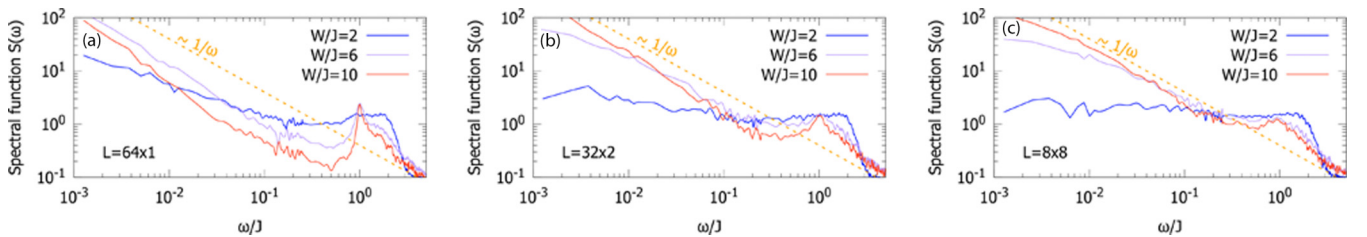

FIG. 6. Spectral function $S(\omega)$ of imbalance for different lattice shapes 64×1 ((a) finite 1D lattice), 32×2 ((b) crossover region between 1D and 2D lattice) and 8×8 ((c) finite 2D lattice). Results represent data for fTWA with disorder strength which varies from $W/J = 2$ to $W/J = 10$. Each line is obtained from averaging over 30 disorder realizations. In fTWA$_{LOC}$ 25 trajectories were simulated for each disorder realization. The rest of the parameters are $V/J = 1$, $J = 0.5$.
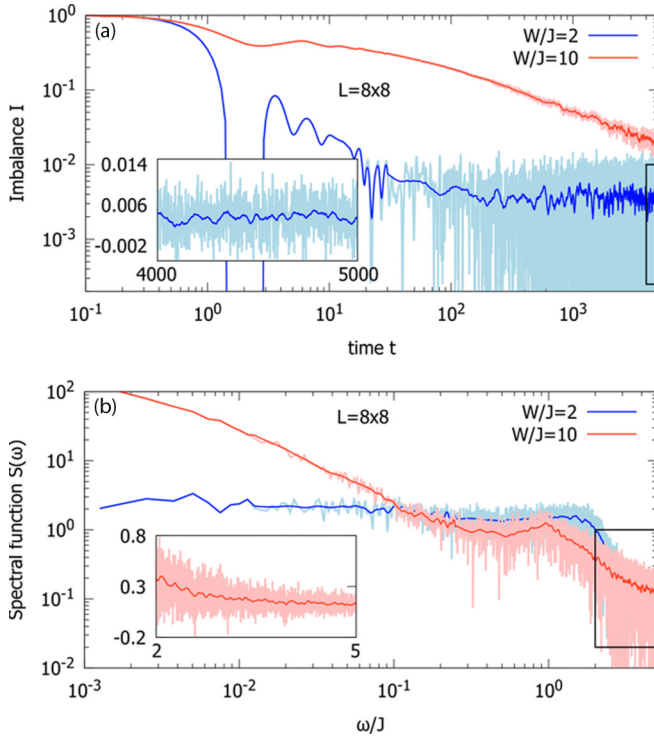
FIG. 7. Example of data for imbalance I and spectral function $S(\omega)$ with and without filtering of the noise. Panel (a) corresponds to data in the inset of Fig. 5(a), and panel (b) corresponds to the data from Fig. 6(c). In the insets, a detailed comparison of the original and filtered data is plotted without a log-log scale.

V. SUMMARY

In this work we analyze the slow dynamics of spinless interacting fermions on one- and two-dimensional lattices with disorder. Using fTWA and exact simulations we show that the fTWA method gives an upper bound on the relaxations rates at single disorder realization. We exploit this method to analyze fermionic dynamics for up to 64 lattice sites at half filling and for times of order $\mathcal{O}(10^3)$, obtaining bounds on the quantum dynamics of the system.

Moreover, we demonstrate that fTWA exhibits $1/\omega$ behavior of the spectral function in one and two dimensions,
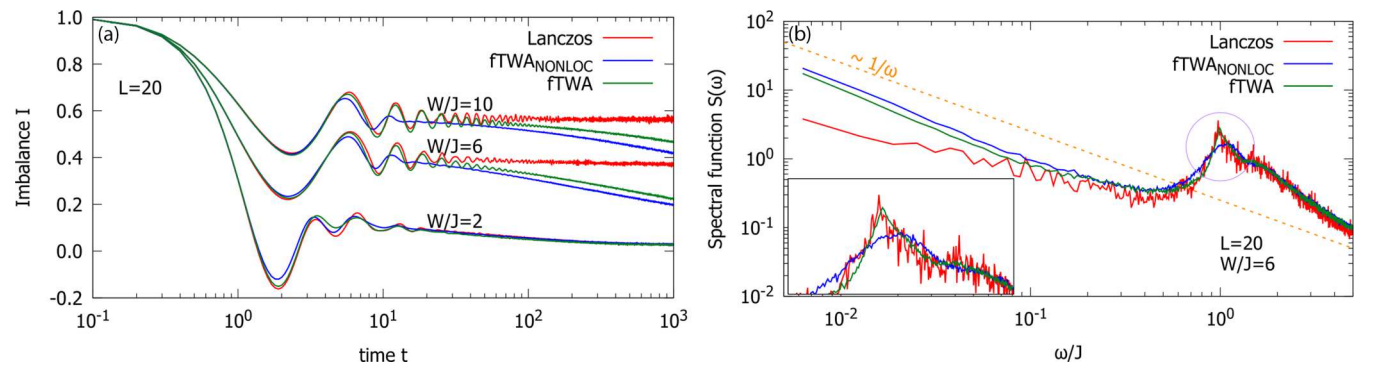
suggesting the universality of such behavior in strongly disordered systems. The $1/\omega$ feature is a footprint of logarithmic-in-time imbalance decay which was previously observed also in one-dimensional disorder systems [28,42,78,79]. Analyzing the spectral functions in 1D systems we observe that, upon increasing the system size, results from the Lanczos method drift to the fTWA results, while the size dependence in fTWA is negligible. The origin of this unexpected feature remain an open problem. It deserves further investigations also for other quantum systems.

APPENDIX A: PHASE SPACE REPRESENTATION OF SPINLESS FERMIONIC HAMILTONIAN

We check that adding to the Hamiltonian $\hat{H}$ the effective local interaction term $V \sum_i (\hat{n}_i - 1/2)^2$ [Eq. (1)] leads to the significant improvement of fTWA at early times up to order $\mathcal{O}(10)$. At later times improvement of fTWA is also visible. We present these results in Fig. 8(a), in which results without local interaction term are denoted by fTWA$_{\text{NONLOC}}$. The explanation of this behavior is the following. In Ref. [75] it was shown that, for the long-range interacting model, fTWA dynamics can be significantly improved by including the local interaction term between the same fermion species. This is because the semiclassical dynamics becomes exact in the long-range limit only if this term is explicitly included in the equations of motion. Formally it means that the term $V \sum_i (\hat{n}_i - 1/2)^2$, which is irrelevant in the exact dynamics

FIG. 8. Comparison of fTWA and fTWA$_{\text{NONLOC}}$ for time-dependent imbalance $I(t)$ (a) and its spectral function $S(\omega)$ (b). There are 500 trajectories in both fTWA and fTWA$_{\text{NONLOC}}$ (green and blue lines, respectively). The inset in (b) shows a sharp peak around $\omega/J = 1$ frequency. The rest of the parameters in (a) and (b) correspond to Figs. 1 and 3(b), respectively.
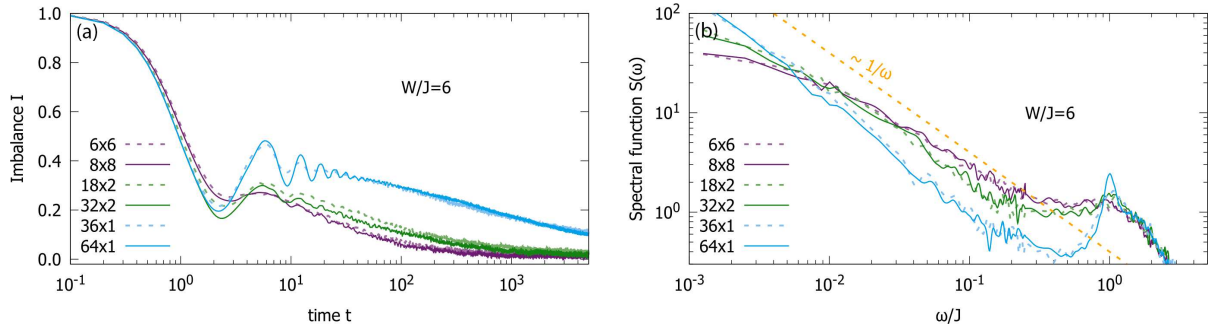
FIG. 9. Finite-size effects in fTWA for time-dependent imbalance (a) and spectral function $S(\omega)$ (b) for different lattice topologies with 64 lattice sites and 36 lattice sites. Presented data represent lattices with shapes 6×6, 18×2, and 36×1, where $W/J = 6$ disorder strength was used. Each simulated curve is averaged over 75 disorder realizations. In fTWA there are 25 trajectories for each disorder realization. The rest of the parameters are the same as in Fig. 5.

(because it is proportional to the total number of particles), has to be implemented in the phase space description as $V \sum_i \rho_{ii}^2$. Such a term introduces nonlinearity in the equations of motion needed for recovery of exact long-range behavior within fTWA.

Moreover, one can also give an alternative explanation of the $V \sum_i \rho_{ii}^2$ term's presence in the semiclassical representation. Namely, such a term naturally appears in the $su(N)$ invariant Hubbard model, and it was recently studied in the large-N flavor limit within fTWA [76].

In the end, it is also worth stressing that fTWA perfectly recovers imbalance oscillations at initial times, which are seen as sharp peaks around $\omega/J = 1$ [92] and which do not appear in the standard fTWA$_{NONLOC}$ description [see Figs. 8(a) and 8(b)].

APPENDIX B: FINITE-SIZE EFFECTS

In Secs. III and IV we analyze imbalance function and its Fourier transform for the system at half filling with 64 lattice sites. In order to analyze finite-size effects we compare dimensional crossover with simulations for 32 lattice sites in Fig. 9. We conclude that, for disorder strength $W/J = 6$, finite-size effects have a small impact on the analyzed dynamics in this paper. We expect that the finite-size effect can be more important for weaker disorder strength. However, main results of our work concern strong disorder, so we omit this analysis.

APPENDIX C: NOISE ANALYSIS

For the sake of clarity of the presentation in Figs. 4–9 we use noise filtering implemented by the convolution of the numerical data with the Kaiser window. Denoting the original and filtered data points by $\mathcal{O}^{original}(x_i)$ and $\mathcal{O}^{filtered}(x_i)$, respectively, the convolution is defined as

$$\mathcal{O}^{filtered}(x_i) = \frac{1}{\mathcal{N}} \sum_{x_j = y_-(i)}^{y_+(i)} \mathcal{O}^{original}(x_j) w(x_i - x_j), \quad \text{(C1)}$$

where $y_\pm(i) = x_i \pm \Delta x(M-1)/2$, the number M is an (odd) integer which set the window width, and the Kaiser window

has the form

$$w(x_i) = I_0\left(\alpha \sqrt{1 - \frac{4x_i^2}{\Delta x^2(M-1)^2}} \right) \Bigg/ I_0(\alpha). \quad \text{(C2)}$$

The normalization condition $\mathcal{N}$ is given by

$$\mathcal{N} = \sum_{x_i = -\Delta x(M-1)/2}^{\Delta x(M-1)/2} w(x_i). \quad \text{(C3)}$$

Moreover, $\mathcal{O}$ corresponds to the imbalance (I) or spectral function (S) and $x_i = i\Delta x$ is a discrete variable representing time t or frequency ω, respectively (Δx denotes the step in the numerical data). I_0 is the modified zeroth-order Bessel function. The time window, tuned by parameters M, α, was correspondingly larger for later times in order to smooth the noise more efficiently (e.g., $M = 401$, $\alpha = 2$, $\Delta t = 0.1$ are chosen for imbalance and $M = 101$, $\alpha = 10$, $\Delta\omega = 2\pi/T_{total}$ for the spectral function, where T_{total} is the total time of simulations). To take into account the boundary effects of the convolution defined in Eq. (C1), original data at boundaries were extended by its mirror reflection. To inspect how noise filtering works at later times, see insets in Figs. 7(a) and 7(b).
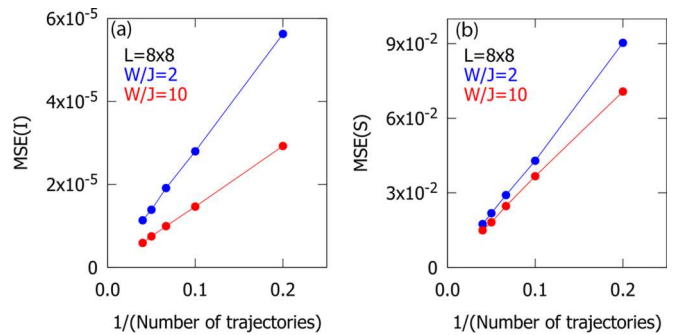

FIG. 10. The mean squared error calculated between the original and filtered data [see Eq. (C4)] for (a) imbalance $I(t)$ and (b) spectral function $S(\omega)$ when the inverse number of trajectories is varied. The data correspond to those presented in Fig. 7 with the same color style of the curves.

Next, we show that a significant part of the noise comes from the finite sampling of the initial Wigner function. To this end we calculate the mean squared error (MSE) between the original and filtered data where the number of trajectories is increased,

$$\text{MSE}(\mathcal{O}) = \frac{1}{N} \sum_{i=1}^{N} [\mathcal{O}^{\text{original}}(x_i) - \mathcal{O}^{\text{filtered}}(x_i)]^2, \quad \text{(C4)}$$

where N is the number of data points. The MSE is calculated in the whole range of available data in a time and frequency domain. From Fig. 10 it is easy to notice that a filtered signal is subsequently approached by original data when the number of sampled trajectories is increased. We also checked that further increasing the number of trajectories does not change the filtered signal.

[1] D. Basko, I. Aleiner, and B. Altshuler, Ann. Phys. (NY) **321**, 1126 (2006).

[2] V. Oganesyan and D. A. Huse, Phys. Rev. B **75**, 155111 (2007).

[3] C. Monthus and T. Garel, Phys. Rev. B **81**, 134202 (2010).

[4] D. J. Luitz, N. Laflorencie, and F. Alet, Phys. Rev. B **91**, 081103(R) (2015).

[5] F. Andraschko, T. Enss, and J. Sirker, Phys. Rev. Lett. **113**, 217201 (2014).

[6] P. Ponte, Z. Papić, F. Huveneers, and D. A. Abanin, Phys. Rev. Lett. **114**, 140401 (2015).

[7] A. Lazarides, A. Das, and R. Moessner, Phys. Rev. Lett. **115**, 030402 (2015).

[8] R. Vasseur, S. A. Parameswaran, and J. E. Moore, Phys. Rev. B **91**, 140202(R) (2015).

[9] M. Serbyn, Z. Papić, and D. A. Abanin, Phys. Rev. B **90**, 174302 (2014).

[10] D. Pekker, G. Refael, E. Altman, E. Demler, and V. Oganesyan, Phys. Rev. X **4**, 011052 (2014).

[11] E. J. Torres-Herrera and L. F. Santos, Phys. Rev. B **92**, 014208 (2015).

[12] M. Távora, E. J. Torres-Herrera, and L. F. Santos, Phys. Rev. A **94**, 041603(R) (2016).

[13] C. R. Laumann, A. Pal, and A. Scardicchio, Phys. Rev. Lett. **113**, 200405 (2014).

[14] D. A. Huse, R. Nandkishore, and V. Oganesyan, Phys. Rev. B **90**, 174202 (2014).

[15] S. Gopalakrishnan, K. R. Islam, and M. Knap, Phys. Rev. Lett. **119**, 046601 (2017).

[16] J. Hauschild, F. Heidrich-Meisner, and F. Pollmann, Phys. Rev. B **94**, 161109(R) (2016).

[17] J. Herbrych, J. Kokalj, and P. Prelovšek, Phys. Rev. Lett. **111**, 147203 (2013).

[18] J. Z. Imbrie, Phys. Rev. Lett. **117**, 027201 (2016).

[19] R. Steinigeweg, J. Herbrych, F. Pollmann, and W. Brenig, Phys. Rev. B **94**, 180401(R) (2016).

[20] J. Herbrych and J. Kokalj, Phys. Rev. B **95**, 125129 (2017).

[21] R. K. Panda, A. Scardicchio, M. Schulz, S. R. Taylor, and M. Žnidarič, Europhys. Lett. **128**, 67003 (2020).

[22] P. Sierant, D. Delande, and J. Zakrzewski, Phys. Rev. Lett. **124**, 186601 (2020).

[23] P. Sierant, M. Lewenstein, and J. Zakrzewski, Phys. Rev. Lett. **125**, 156601 (2020).

[24] A. Morningstar, L. Colmenarez, V. Khemani, D. J. Luitz, and D. A. Huse, Phys. Rev. B **105**, 174205 (2022).

[25] D. Abanin, J. Bardarson, G. De Tomasi, S. Gopalakrishnan, V. Khemani, S. Parameswaran, F. Pollmann, A. Potter, M. Serbyn, and R. Vasseur, Ann. Phys. **427**, 168415 (2021).

[26] J. Šuntajs, J. Bonča, T. Prosen, and L. Vidmar, Phys. Rev. E **102**, 062144 (2020).

[27] J. Šuntajs, J. Bonča, T. Prosen, and L. Vidmar, Phys. Rev. B **102**, 064207 (2020).

[28] D. Sels and A. Polkovnikov, Phys. Rev. E **104**, 054105 (2021).

[29] D. Sels, Phys. Rev. B **106**, L020202 (2022).

[30] D. Sels and A. Polkovnikov, arXiv:2105.09348.

[31] M. Žnidarič, T. Prosen, and P. Prelovšek, Phys. Rev. B **77**, 064426 (2008).

[32] J. H. Bardarson, F. Pollmann, and J. E. Moore, Phys. Rev. Lett. **109**, 017202 (2012).

[33] J. A. Kjäll, J. H. Bardarson, and F. Pollmann, Phys. Rev. Lett. **113**, 107204 (2014).

[34] M. Serbyn, Z. Papić, and D. A. Abanin, Phys. Rev. X **5**, 041047 (2015).

[35] D. J. Luitz, N. Laflorencie, and F. Alet, Phys. Rev. B **93**, 060201(R) (2016).

[36] M. Serbyn, Z. Papić, and D. A. Abanin, Phys. Rev. Lett. **110**, 260601 (2013).

[37] S. Bera, H. Schomerus, F. Heidrich-Meisner, and J. H. Bardarson, Phys. Rev. Lett. **115**, 046603 (2015).

[38] E. Altman and R. Vosk, Annu. Rev. Condens. Matter Phys. **6**, 383 (2015).

[39] K. Agarwal, S. Gopalakrishnan, M. Knap, M. Müller, and E. Demler, Phys. Rev. Lett. **114**, 160401 (2015).

[40] S. Gopalakrishnan, M. Müller, V. Khemani, M. Knap, E. Demler, and D. A. Huse, Phys. Rev. B **92**, 104202 (2015).

[41] M. Žnidarič, A. Scardicchio, and V. K. Varma, Phys. Rev. Lett. **117**, 040601 (2016).

[42] M. Mierzejewski, J. Herbrych, and P. Prelovšek, Phys. Rev. B **94**, 224207 (2016).

[43] Y. Bar Lev and D. R. Reichman, Phys. Rev. B **89**, 220201(R) (2014).

[44] Y. Bar Lev, G. Cohen, and D. R. Reichman, Phys. Rev. Lett. **114**, 100601 (2015).

[45] O. S. Barišić, J. Kokalj, I. Balog, and P. Prelovšek, Phys. Rev. B **94**, 045126 (2016).

[46] J. Bonča and M. Mierzejewski, Phys. Rev. B **95**, 214201 (2017).

[47] P. Bordia, H. Lüschen, S. Scherg, S. Gopalakrishnan, M. Knap, U. Schneider, and I. Bloch, Phys. Rev. X **7**, 041047 (2017).

[48] P. Sierant, D. Delande, and J. Zakrzewski, Phys. Rev. A **95**, 021601(R) (2017).

[49] I. V. Protopopov and D. A. Abanin, Phys. Rev. B **99**, 115111 (2019).

[50] M. Schecter, T. Iadecola, and S. Das Sarma, Phys. Rev. B **98**, 174201 (2018).

[51] J. Zakrzewski and D. Delande, Phys. Rev. B **98**, 014203 (2018).

[52] A. Chandran, V. Khemani, C. R. Laumann, and S. L. Sondhi, Phys. Rev. B **89**, 144201 (2014).

[53] A. C. Potter and R. Vasseur, Phys. Rev. B **94**, 224206 (2016).

[54] P. Prelovšek, O. S. Barišić, and M. Žnidarič, Phys. Rev. B **94**, 241104(R) (2016).

[55] I. V. Protopopov, W. W. Ho, and D. A. Abanin, Phys. Rev. B **96**, 041122(R) (2017).

[56] A. J. Friedman, R. Vasseur, A. C. Potter, and S. A. Parameswaran, Phys. Rev. B **98**, 064203 (2018).

[57] Y. B. Lev and D. R. Reichman, Europhys. Lett. **113**, 46001 (2016).

[58] X. Li, D.-L. Deng, Y.-L. Wu, and S. Das Sarma, Phys. Rev. B **95**, 020201(R) (2017).

[59] D. J. Luitz and Y. Bar Lev, Phys. Rev. Lett. **117**, 170404 (2016).

[60] D. J. Luitz and Y. Bar Lev, Annalen der Physik **529**, 1600350 (2017).

[61] M. Kozarzewski, P. Prelovšek, and M. Mierzejewski, Phys. Rev. Lett. **120**, 246602 (2018).

[62] P. Prelovšek and J. Herbrych, Phys. Rev. B **96**, 035130 (2017).

[63] Y. B. Lev, D. M. Kennes, C. Klöckner, D. R. Reichman, and C. Karrasch, Europhys. Lett. **119**, 37003 (2017).

[64] P. Prelovšek, J. Bonča, and M. Mierzejewski, Phys. Rev. B **98**, 125119 (2018).

[65] K. Agarwal, E. Altman, E. Demler, S. Gopalakrishnan, D. A. Huse, and M. Knap, Annalen der Physik **529**, 1600326 (2017).

[66] H. P. Lüschen, P. Bordia, S. Scherg, F. Alet, E. Altman, U. Schneider, and I. Bloch, Phys. Rev. Lett. **119**, 260401 (2017).

[67] J.-y. Choi, S. Hild, J. Zeiher, P. Schauss, A. Rubio-Abadal, T. Yefsah, V. Khemani, D. A. Huse, I. Bloch, and C. Gross, Science **352**, 1547 (2016).

[68] B. Chiaro, C. Neill, A. Bohrdt, M. Filippone, F. Arute, K. Arya, R. Babbush, D. Bacon, J. Bardin, R. Barends, S. Boixo, D. Buell, B. Burkett, Y. Chen, Z. Chen, R. Collins, A. Dunsworth, E. Farhi, A. Fowler, B. Foxen *et al.*, Phys. Rev. Res. **4**, 013148 (2022).

[69] S. S. Kondov, W. R. McGehee, W. Xu, and B. DeMarco, Phys. Rev. Lett. **114**, 083002 (2015).

[70] M. Mierzejewski, M. Środa, J. Herbrych, and P. Prelovšek, Phys. Rev. B **102**, 161111(R) (2020).

[71] A. Štrkalj, E. V. H. Doggen, and C. Castelnovo, Phys. Rev. B **106**, 184209 (2022).

[72] S. M. Davidson, D. Sels, and A. Polkovnikov, Ann. Phys. (NY) **384**, 128 (2017).

[73] S. M. Davidson, Ph.D. thesis, Boston University, 2017, https://open.bu.edu/handle/2144/24091.

[74] M. Schmitt, D. Sels, S. Kehrein, and A. Polkovnikov, Phys. Rev. B **99**, 134301 (2019).

[75] A. S. Sajna and A. Polkovnikov, Phys. Rev. A **102**, 033338 (2020).

[76] A. Osterkorn and S. Kehrein, arXiv:2007.05063.

[77] A. Osterkorn and S. Kehrein, Phys. Rev. B **106**, 214318 (2022).

[78] M. Serbyn, Z. Papić, and D. A. Abanin, Phys. Rev. B **96**, 104201 (2017).

[79] L. Vidmar, B. Krajewski, J. Bonča, and M. Mierzejewski, Phys. Rev. Lett. **127**, 230603 (2021).

[80] L. M. Ward and P. E. Greenwood, Scholarpedia **2**, 1537 (2007).

[81] In comparison to Ref. [72], we include an extra imaginary unit i factor into the definition of the Poisson brackets in Eqs. (2) and (4).

[82] A. Polkovnikov, Ann. Phys. (NY) **325**, 1790 (2010).

[83] T. J. Park and J. C. Light, J. Chem. Phys. **85**, 5870 (1986).

[84] M. Mierzejewski and P. Prelovšek, Phys. Rev. Lett. **105**, 186405 (2010).

[85] M. Schreiber, S. S. Hodgman, P. Bordia, H. P. Lüschen, M. H. Fischer, R. Vosk, E. Altman, U. Schneider, and I. Bloch, Science **349**, 842 (2015).

[86] P. Bordia, H. P. Lüschen, S. S. Hodgman, M. Schreiber, I. Bloch, and U. Schneider, Phys. Rev. Lett. **116**, 140401 (2016).

[87] J. Smith, A. Lee, P. Richerme, B. Neyenhuis, P. W. Hess, P. Hauke, M. Heyl, D. A. Huse, and C. Monroe, Nat. Phys. **12**, 907 (2016).

[88] H. P. Lüschen, P. Bordia, S. S. Hodgman, M. Schreiber, S. Sarkar, A. J. Daley, M. H. Fischer, E. Altman, I. Bloch, and U. Schneider, Phys. Rev. X **7**, 011034 (2017).

[89] O. L. Acevedo, A. Safavi-Naini, J. Schachenmayer, M. L. Wall, R. Nandkishore, and A. M. Rey, Phys. Rev. A **96**, 033604 (2017).

[90] J. Wurtz, A. Polkovnikov, and D. Sels, Ann. Phys. (NY) **395**, 341 (2018).

[91] http://wcss.pl.

[92] M. Kozarzewski, P. Prelovšek, and M. Mierzejewski, Phys. Rev. B **93**, 235151 (2016).